Noncontact Dipole Effects on Channel Permeation. IV. Kinetic Model of 5F-Trp$_{13}$ Gramicidin A Currents

Nephi Thompson,*‡ Gina Thompson,† Chad D. Cole,‡ Myriam Cotten,§ Timothy A. Cross,§ and David D. Busath‡

*Department of Physics and Astronomy, †Department of Mathematics, and ‡Department of Zoology and Center for Neuroscience, Brigham Young University, Provo, Utah 84602, and §Center for Interdisciplinary Magnetic Resonance at the National High Magnetic Field Laboratory, Institute of Molecular Biophysics and Department of Chemistry, Florida State University, Tallahassee, Florida 32306, USA

ABSTRACT Nonlinear least squares fitting was used to assign rate constants for the three-barrier, two-site, double-occupancy, single-filing kinetic model for previously reported current–voltage relations of (5F-Indole)Trp$_{13}$ gramicidin A and gramicidin A channels (Busath et al., *Biophys. J.*, 1998, 75:2830–2844). By judicious coupling of parameters, it was possible to reduce the parameter space from 64 parameters to 24, and a reasonable fit consistent with other experimental data was obtained. The main features of the fit were that fluorination increased the rate constant for translocation by a factor of 2.33, consistent with a free energy change in the translocation barrier of −0.50 kcal/mol, and increased first-ion binding affinity by a factor of 1.13, primarily by decreasing the first-ion exit rate constant. The translocation rate constant was 5.62 times slower in diphytanoyl phosphatidylcholine (DPhPC) bilayers than in monoolein (GMO) bilayers (coupled for the four combinations of peptide and salt), suggesting a 44.2-mV difference in the projection of the interfacial dipole into the channel. Thus fluorination caused increased currents in DPhPC bilayers, where a high interfacial dipole potential makes translocation more rate limiting because the translocation barrier was reduced, and decreased currents in GMO bilayers, where ion exit or entry is rate limiting because these barriers were increased.

INTRODUCTION

This paper is part of a series devoted to analysis of how dipoles near the permeation pathway regulate ion flow in ion channels. The results are expected to be useful for interpreting channel permeability as a reflection of underlying structural details and other determinants of potential energy such as charge distribution on side chains in close proximity to the channel interior. Here, we report modeling of the data published in the first paper of this series (Busath et al., 1998) using a typical set of parameters for the three-barrier, two-site (3B2S) single filing kinetic model, the simplest kinetic model that accounts for single filing in a double-occupancy channel (Hladky and Haydon, 1984).

Discrete-step rate theory or kinetic theory, electrodiffusive continuum theory, and Brownian dynamics have been applied extensively to predict ionic currents through gramicidin channels in lipid membranes (Busath, 1993). Debate continues over the respective weaknesses of these theories, namely that the kinetic model is best suited for high narrow barriers, whereas continuum theory fails to adequately represent the interactions between ions in a single-file pore (Busath, 1993; Cooper et al., 1988; Hladky, 1999; also see editorials and articles in *J. Gen. Physiol.* Vol. 113 Num. 4 and Vol. 114 Num. 4). However, in one study of gramicidin permeation data, rate and continuum theory were approximately equal in data-fitting capacity (Levitt, 1982).

More complex rate theory models have often been used, including parameters for a preliminary external binding site (Eisenman and Sandblom, 1983), diffusion limitation and interfacial polarization effects on entry (Andersen, 1983a,b,c; Becker et al., 1992), different voltage dependencies for double occupancy (Urban and Hladky, 1979), and modified voltage dependence for translocation (Hladky, 1999; Urban and Hladky, 1979; McBride, 1981), but no clear necessity for these complications has emerged (Becker et al., 1992; McBride, 1981). In particular, diffusion limitations and interfacial polarization are well simulated by a single-entry rate constant (Hladky, 1984; Becker et al., 1992), and are expected to be most problematic at low ion concentrations and high membrane potentials (Hainsworth and Hladky, 1987), neither of which was examined here.

This data set consists of 320 data points, each representing the mean of three or more experiments. Eight different experimental paradigms are represented (2 ions × 2 lipids × 2 peptides). We arbitrarily chose the gramicidin A (gA) potassium currents in diphytanoyl phosphatidylcholine (DPhPC) bilayers as the base paradigm and considered how each of the other paradigms relate to it. We assume that a rate constant in a paradigm differing in only one way (lipid, ion, or peptide) from the base paradigm is independently related to the rate constant in the base paradigm by a difference in transition-state free energy or in collision rate, and thus differs by a factor specific to that paradigm change. The coupling constants were allowed to vary as parameters, but reduced the number of ways that rate constants could vary among the eight paradigms from 8 to 4.

The fitted parameters, which were satisfactorily determined by the data set, were compared to theoretical expec-

Received for publication 3 January 2000 and in final form 31 May 2001.

Address reprint requests to David Busath, Department of Zoology and Center for Neuroscience, Brigham Young University, Provo, UT 84602. Tel.: 801-378-8753; Fax: 801-378-7423; E-mail: david_busath@byu.edu.

0006-3495/01/09/1245/10 $2.00

tations and found to be reasonable in all cases. In particular, the coupling constant associated with fluorination of Trp_{13} in gA, (the fluorination coupling constant), was found to be consistent with expectations from molecular modeling (Dorigo et al., 1999; Anderson et al., 2001). In addition, the results support the interpretation that fluorination reduces conductance in GMO bilayers (Busath et al., 1998) because the interfacial dipole potential (and therefore the barrier to translocation) is relatively low. It was previously speculated that entry would be inhibited by the increased positive end of the dipole upon fluorination (Busath et al., 1998). However, analysis of Eadie–Hofstee plots using the 3B2S model indicates that exit from the doubly-occupied pore, rather than entry, is more rate limiting in the intermediate concentration range, which occurs at higher concentrations in GMO because of the low barrier to translocation. Here we conclude from our data fitting that inhibition of exit, rather than entry, is rate limiting in GMO bilayers in the 0.1–1.0 M concentration range. These results have appeared in preliminary form (Thompson et al., 1999) and are expected to form the foundation for eventual analysis of a yet broader data set based on seven additional fluorinated peptides (C. D. Cole, A. Frost, M. Cotten, T. A. Cross, and D. D. Busath, submitted for publication).

METHODS

Measured currents and errors

The data for the fit were reported in graphical form in Busath et al. (1998) and are available freely on the World Wide Web at http://bioag.byu.edu/zoology/gramicidin/index.html. Errors associated with the individual data points were used indirectly as follows. Each data point consists of the mean of $N = 3–4$ experiments and its standard error estimated as $SD \cdot N^{0.5}$, where SD is the (N-1 type) standard deviation of the average main peak current in the 3–4 experiments. These standard errors showed considerable variation due to small sample size. However, the large number of data points (320) allowed an improved estimate of the error through statistical evaluation. The 320 standard errors were examined for their relationship to mean channel current to determine the extent to which they were proportional errors as opposed to constant errors (Bevington, 1969). It was found that the standard errors for the 320 experiments were randomly distributed, but correlated with the mean channel current, $\bar{\imath}$ (Fig. 1). The weights used for fitting were based on the least-squares fit of a line to these errors, which yielded the equation

$$W(\text{pA}) = 0.0143\bar{\imath}(\text{pA}) + 0.0026\ \text{pA}. \qquad (1)$$

Model description

Figure 2 illustrates the state diagram for the 3B2S model (Hladky and Haydon, 1984). It has four states that are symbolized as 00 for the empty channel, 10 for the singly occupied channel with an ion in the left binding site, 01 for the singly occupied channel with an ion in the right binding site, and 11 for the doubly occupied channel. Ten rate constants describe the allowed transitions between the four states. Primed rate constants denote movement left to right, and double primed rate constants denote movement right to left. The rate constants all have exponential voltage dependencies that depend on entry, exit, and translocation electrical distances. These are

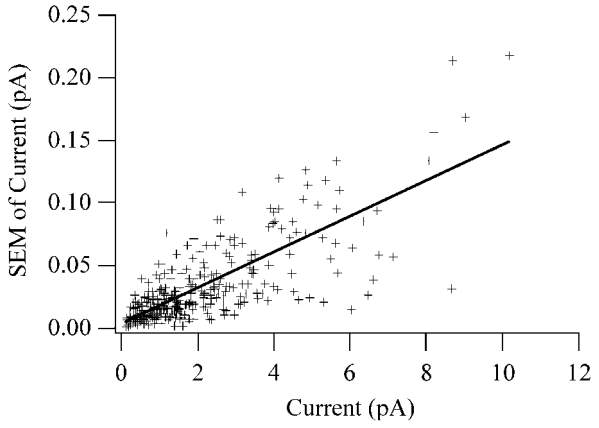

FIGURE 1 Standard errors from 3–4 experiments plotted against mean channel current for the 320 data points fitted here. The standard errors scatter about the solid line, the least squares fit, which was used to calculate the weights for Eq. 2.

defined as α_1, the distance from "bulk" solution to the peak of the "entry barrier" and α_2, the distance from the bulk to the binding site. Due to bilateral symmetry, α_3, the distance from the bulk to the peak of the translocation barrier, is fixed at 0.5. Second-ion entry and exit voltage dependencies were set equal to those for the first ion for simplicity.

Figure 3 is a rate constant representation profile (Andersen, 1999) for an ion passing through a two-site channel, shown with the corresponding rate constants from the state diagram. The profile in Fig. 3 is a schematic profile that is not intended to represent our final fitted parameters. The profile for a singly occupied channel is depicted with the solid line, and the energetics of binding with the opposite site occupied are depicted with the dashed line. The rate constants are related to the change in free energy among the different states. The profile derives from the notion that Eyring rate theory can be used to relate the rate constants to the heights of the barriers and that the transmission coefficient is always one. These premises are known to be unrealistic in gramicidin channels. The breadth of the translocation barrier precludes the high transmission coefficient and the entry step is diffusion limited rather than energy-barrier limited (Cooper et al., 1988). But changes in rate constants can reasonably be ascribed to energy changes in the rate constant representation profile, and the relationships between rate constants and their voltage dependencies, when established using the profile, assure that microscopic reversibility is satisfied. Thus the profile is a convenient way to quantitatively display the relative significance of the rate constants. For example, A′ (the rate constant describing ion entry into

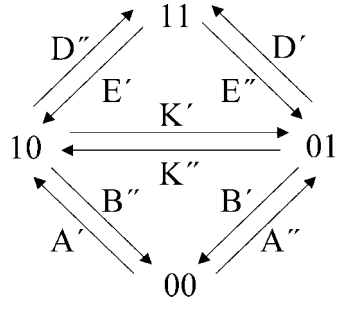

FIGURE 2 The four-state model for permeation used here. Channel site occupancy is symbolized by 1, vacancy by 0 (Hlakdy and Haydon, 1984). Rate constants for movement from left to right are primed and from right to left are double primed.

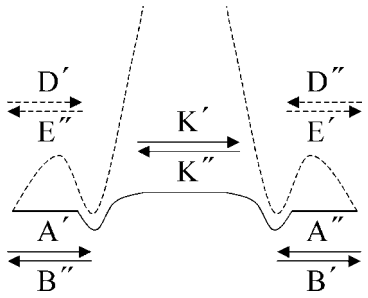

FIGURE 3 A schematic rate constant representation profile (Andersen, 1999) of the channel shown with corresponding rate constants. The solid line represents the energy profile of the unoccupied channel and the dashed line represents the energy profile of a singly occupied channel. Translocation through a channel occupied on the opposite side is disallowed (Fig. 2).

the unoccupied channel from the left side) is used here to represent the effective rate of the processes of diffusion up to the channel, outer-sphere complex formation, ion dehydration, and binding. The entry barrier, then, is not a free energy barrier but an artifice used to yield the correct rate constant via Eyring rate theory. Any change in the free energy barrier to entry is accurately represented as a change in the entry barrier height. Similar arguments can be made for the relationships between changes in energies and the other rate constants. In the case of translocation, the breadth of the peak may preclude the assumptions required for the use of Eyring rate theory, but, from Kramers' theory (Kramers, 1940), it is clear that electrodiffusion across a broad barrier simulated with the Nernst–Planck formalism yields the same relationship between proportionate change in rate constant and change in barrier height. Therefore, these energy considerations formed the basis for developing the coupling constants.

Parameter coupling

For homodimeric channels formed by gA and (5F-Indole)Trp$_{13}$ gramicidin A (5F-Trp$_{13}$ gA), the symmetry is such that the primed rate constants differ from the double primed rate constants by only a voltage-dependence factor. When we refer to specific rate constants hereafter, they will be expressed without primes to represent the zero-voltage rate constant. The voltage dependence of coupling is handled separately.

To reduce the degrees of freedom in the fit, we define a set of coupling constants to interrelate the rate constants. For instance, we assume that the Na^+ entry rate should be proportional to Na^+ mobility in bulk solution for both lipids and both peptides (although other factors such as dehydration will come into play as well) and, likewise, that the K^+ entry rate should be proportional to K^+ mobility. Therefore, the entry rate constants for the two ions should always differ by a constant factor, namely the ratio of their bulk mobilities. The other factors were also expected to be multiplicative because they derive from free energy differences such as the interfacial dipole potential differences for the lipids, the binding affinity and diffusion coefficient differences for the ions, and the electrostatic effects of fluorination, all of which are expected to affect a rate constant through a Boltzmann factor.

The five rate constant parameters for gA in DPhPC and K^+ were our basis set. Rate constants for the other experimental paradigms were coupled to them through the coupling constants. For example, suppose the K^+ first-ion exit rate for gA in a DPhPC bilayer (B^{Basis}) is exponentially related to an exit barrier G_{gA}^{Exit} such that $B^{Basis} = J\exp(-G_{gA}^{Exit})$ where J is a proportionality constant. 5F-Trp$_{13}$ fluorination changes G_{gA}^{Exit} by ΔG_{FgA}^{Exit} such that $G_{FgA}^{Exit} = G_{FgA}^{Exit} + \Delta G_{FgA}^{Exit}$ and $B^{FgA} = J\exp(-G_{FgA}^{Exit}) = J\exp[-(G_{gA}^{Exit} + \Delta G_{FgA}^{Exit})] = J\exp(-G_{gA}^{Exit}) \cdot \exp(-\Delta G_{FgA}^{Exit})$. We then define a coupling constant $C_B^F = \exp(-\Delta G_{FgA}^{Exit})$ to represent the energetic consequence of 5F-Trp$_{13}$ fluorination on the exit barrier. The K^+ exit rate for the 5F-Trp$_{13}$ fluorinated peptide in DPhPC bilayers is given by $B^{FgA} = B^{Basis} \cdot C_B^F$. We assume that the energetic consequence would be the same when comparing the rate constant for fluorinated and native peptides, in K^+ or Na^+, and in DPhPC or GMO bilayers. This same procedure is applied for each experimental paradigm.

TABLE 1 Rate constant coupling rationale illustration for first-ion exit rate constant, B

	gA	5F-Trp$_{13}$ gA
DPhPC/K^+	B^{Basis}	$B^{Basis} \cdot C_B^F$
DPhPC/Na^+	$B^{Basis} \cdot C_B^{Ion}$	$B^{Basis} \cdot C_B^{Ion} \cdot C_B^F$
GMO/K^+	$B^{Basis} \cdot C_B^{Lipid}$	$B^{Basis} \cdot C_B^{Lipid} \cdot C_B^F$
GMO/Na^+	$B^{Basis} \cdot C_B^{Ion} \cdot C_B^{Lipid}$	$B^{Basis} \cdot C_B^{Ion} \cdot C_B^{Lipid} \cdot C_B^F$

Table 1 illustrates the coupling constant rationale for B, the first-ion exit rate constant. The two columns represent native gA and 5F-Trp$_{13}$ gA while the rows represent the four experimental paradigms used to study each peptide. The rate constant for a particular paradigm is given by the basis rate constant multiplied by the necessary coupling constants. The example given above is illustrated in the second column of the first row of Table 1. This rationale was used for all five rate constants in our basis set.

A total of 20 rate constants and coupling constants were required to fit all of the data simultaneously. Changing the peptide or the ion was assumed to have no effect on voltage dependency of the rate constants, but two voltage-dependency parameters for each lipid were used. Although the locations of the binding sites may differ for the two ions or the two peptides, we believe that such differences would be small. This assumption was justified by fits in which the voltage dependencies were not constrained and did not change substantially nor affect the quality of the fit (data not shown). However, the voltage dependencies in the two lipids were quite different, perhaps a result of the difference in the shape of the translocation barriers due to the contributions of differing interfacial dipole potentials, or possibly due somehow to differences in the membrane thickness. This leaves a total of 24 parameters. Most of these are reasonably well constrained by previous work, and here we are able to focus primarily on just three parameters, the effects of fluorination on first-ion entry, first-ion exit, and translocation, which are C_A^F, C_B^F, and C_K^F, respectively.

Fitting algorithm and procedures

The data set of 320 points was fit with the final 24 parameters using the Levenberg–Marquardt nonlinear least squares fit algorithm (Press et al., 1986). Goodness of fit was estimated using the Bevington reduced χ^2 (Bevington, 1969),

$$\chi_r^2 = \frac{1}{\nu}\sum_i \frac{1}{W_i^2}[\bar{I}_i - i(x_i)]^2, \qquad (2)$$

where ν is the number of degrees of freedom, i.e., one less than the number of points minus the number of free parameters, i is the ith data point, $i(x_i)$ the prediction of the function for the ith data point given all of the independent variables for that data point, x_i, and W_i is the uncertainty for the ith data point estimated from the linear fit to the standard errors discussed above. For 200 degrees of freedom, a technically acceptable fit ($P > 0.05$) is obtained when $\chi_r^2 < 1.17$ (Bevington, 1969), and slightly lower for our case (295 degrees of freedom). However, values of $\chi_r^2 < 5$ were deemed to be good fits from a subjective viewpoint.

Robustness of the fit was tested by variation of the parameter starting values. First, the parameters were assigned values from previously reported fits and experiments in the literature and allowed to vary until they reached

TABLE 2 Final parameter set

Rate constants for basis set (K^+, gA, DPhPC)				
A^{Basis}	B^{Basis}	K^{Basis}	D^{Basis}	E^{Basis}
1.10×10^8 $M^{-1}s^{-1}$	2.20×10^6 s^{-1}	1.85×10^7 s^{-1}	1.18×10^8 $M^{-1}s^{-1}$	3.17×10^7 s^{-1}
Coupling constants				
C_A^{Lipid}	C_B^{Lipid}	C_K^{Lipid}	C_D^{Lipid}	C_E^{Lipid}
0.77	1.34	5.62	0.98	1.52
C_A^{Ion}	C_B^{Ion}	C_K^{Ion}	C_D^{Ion}	C_E^{Ion}
0.56	7.11	0.46	0.18	0.51
C_A^F	C_B^F	C_K^F	C_D^F	C_E^F
0.94	0.83	2.33	0.90	0.72

a minimum. Second, the fluorination parameters were constrained to quantitatively predicted values and others allowed to vary until they reached a minimum. We then constrained the other parameters and allowed the fluorination parameters to vary until they reached a minimum. This process was repeated until a minimum was reached. Finally, in a third independent fit, the parameters were all started at zero and were allowed to vary until they reached a minimum. All three fitting strategies found the same minimum (i.e., the same final χ_r^2 within two decimal places of accuracy and all parameters the same within ~10%).

RESULTS

The parameter set in Table 2 represents the best fit with a final chi-square value of 3.83 per degree of freedom. The rate constants for the basis set (K^+, gA, DPhPC) are given in the first row of Table 2, and the corresponding coupling constants for change of lipid, ion, and fluorination are given in the second through fourth rows, respectively. The same parameter set was obtained with three different starting sets, indicating that it is robust.

Figure 4 shows the currents measured in DPhPC bilayers with the corresponding theoretical predictions. The fit is qualitatively satisfactory. Most importantly, the theoretical predictions have the same shape as the data IVs and predict self-block (i.e., reduction in conductance at high ion concentrations) in DPhPC bilayers, in close correspondence to the observed currents. Also note that 5F-Trp_{13} gA has a higher conductance than gA in DPhPC bilayers for both K^+ and Na^+ (Busath et al., 1998).

Figure 5 shows the currents measured in GMO bilayers with the corresponding theoretical predictions. This fit is also qualitatively satisfactory and exhibits no self-block, in close correspondence to the observed currents. 5F-Trp_{13} gA in GMO bilayers also has a slight decrease in conductance compared to gA, except at 2M concentrations of K^+ (Busath et al., 1998). These features place fairly strong demands on the 3B2S model, judging from the convergence of the fits.

The best-fit parameter set indicates that fluorination decreases the rate constant of first- and second-ion K^+ exit ($C_B^F = 0.83$; $C_E^F = 0.72$), increases the rate constant of translocation ($C_K^F = 2.33$), and leaves the first- and second-ion K^+ entry rate constants relatively unaffected ($C_A^F = 0.94$; $C_D^F = 0.90$). Similar effects are seen for Na^+, judging by the fact that the same set of fluorination-coupling constants could be used successfully for both Na^+ and K^+. Fluorination does not greatly affect ion–ion interaction in this fit. This result is expected if ion–ion interactions are

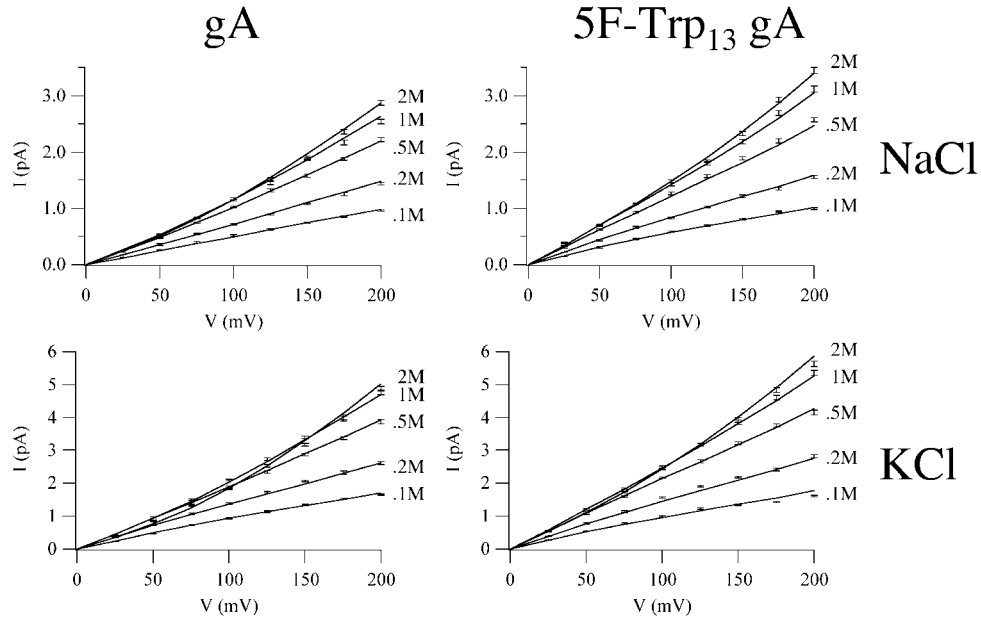

FIGURE 4 IV plots of Na^+ and K^+ currents measured in DPhPC bilayers with the theoretical currents predicted by the 3B2S model. Currents measured in 0.1, 0.2, 0.5, 1.0, and 2.0 M NaCl are displayed in the first row with currents in the same concentrations of KCl in the second. Native gramicidin channels are displayed in the first column with 5F-Trp_{13} gA channels in the second. Data shown as markers with error bars. Theory shown as solid line.

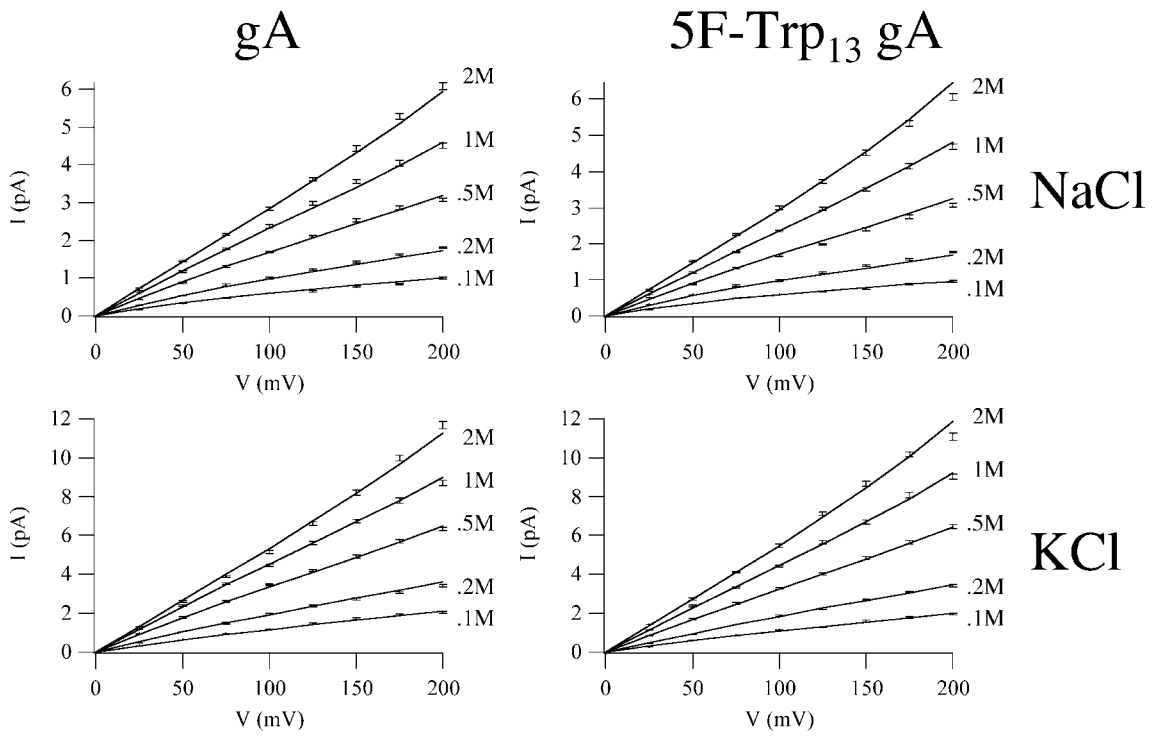

FIGURE 5 IV plots of Na^+ and K^+ currents measured in GMO bilayers with the theoretical currents predicted by the 3B2S model. Same experimental parameters as Fig. 4.

mediated primarily through the waters and peptide backbone, rather than through interactions with the side chains.

Sodium shows a much lower affinity for the channel than potassium, $C_A^{Ion}/C_B^{Ion} = 0.079$ (fixed for both lipids and both peptides by use of coupling constants). This appears to be inappropriate considering NMR studies (Hinton et al., 1988) and water permeability measurements (Wang et al., 1995) that show it to be only slightly lower. However, we have not attempted to modify this parameter in any way. The translocation rate constant is 5.62-fold higher in GMO bilayers than in DPhPC ($C_K^{Lipid} = 5.62$) as expected (Busath et al., 1998) and exit is clearly rate limiting in GMO at intermediate concentrations [$(B^{Basis} \cdot C_B^{Lipid})/(K^{Basis} \cdot C_K^{Lipid}) = 0.028$], but less so in DPhPC, where translocation plays a bigger role ($B^{Basis}/K^{Basis} = 0.12$).

The formal standard errors of the parameters, σ_i, as constrained by the data and data weights, are given by

$$\sigma_i = \sqrt{C_{ii}}, \tag{3}$$

where C is the covariance matrix of the fitted parameters, and i is the ith parameter (Press et al., 1986). For our fit, the uncertainties in the rate constants ($2\sigma_i$) were all $<10\%$ of the parameter values.

A visual demonstration of the goodness-of-fit surface is given in Figure 6, which contains contour plots of the χ^2 surface plotted against two of the fitted parameters with all other parameters held constant. Basis parameter interactions are shown in the first row, and fluorination coupling constant interactions in the second row. Contours of χ^2 are shown at intervals of 5, with the region $\chi^2 \leq 5$ shaded. The surfaces appear smooth and continuous, and the wells appear unambiguous and unique. Parameter correlation appears as an elliptical well with a major axis that has a positive slope for positively correlated parameters or a negative slope for negatively correlated parameters. A and B show little dependence on each other. B and K have a negative correlation with an increase in B compensated by a decrease in K. Small changes in A require large changes in K. The fluorination effects on A and B show little dependence on each other. An increase in the fluorination effect on B is compensated by a decrease in the fluorination effect on K. Small changes in the fluorination effects on A require large changes in the fluorination effects on K. In this fit, the interactions of the basis parameters are similar to the interactions of the fluorination-coupling constants, suggesting some relationship between the two. In the two-parameter views shown in Fig. 6, the goodness-of-fit contour plots contain only single, narrow minima and indicate good constraint of the parameters by the data.

Figure 7 contains the Eadie–Hofstee plots for the DPhPC experimental paradigms and Fig. 8 contains the Eadie–Hofstee plots for the GMO experimental paradigms. Each curve contains a peak on the left and a "foot" on the right. Predicted conductances in the two lipids converge at low

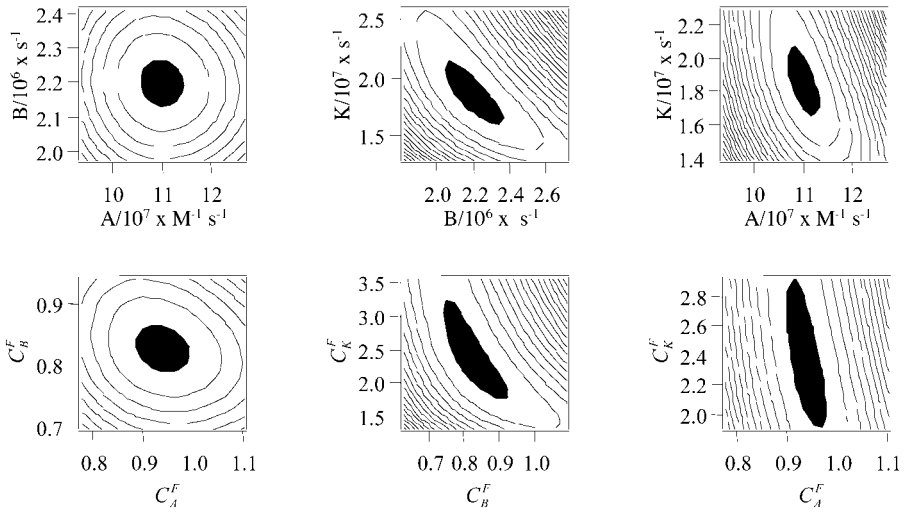

FIGURE 6 Contour plots of the χ_r^2 surface with respect to fitted parameters. Contours of χ_r^2 are shown at intervals of 5, with the region $\chi_r^2 \leq 5$ shaded. The first row contains plots of the rate constants for first-ion entry, first-ion exit, and translocation for the basis set (A^{Basis}, B^{Basis}, K^{Basis}) with all other parameters held constant. The second row contains plots of the coupling constants representing the effect of 5F-Trp_{13} fluorination on first-ion entry, first-ion exit, and translocation (C_A^F, C_B^F, C_K^F) with all other parameters held constant.

activities, i.e., in the foot or K_1 region. Between the ankle and the peak, in the K_2 region, slope changes in the data are poorly approximated by the kinetic model. However, the K^+ paradigms show a more negative slope upon fluorination in both types of bilayers. When conditions are right for a straight segment in this region, (i.e., in the 3B2S model when 2E, 2K $\gg$ Da $\gg$ B), the slope is given by (Hladky and Haydon, 1984)

$$K_2 = \frac{-2KE}{D(K + E)}. \quad (4)$$

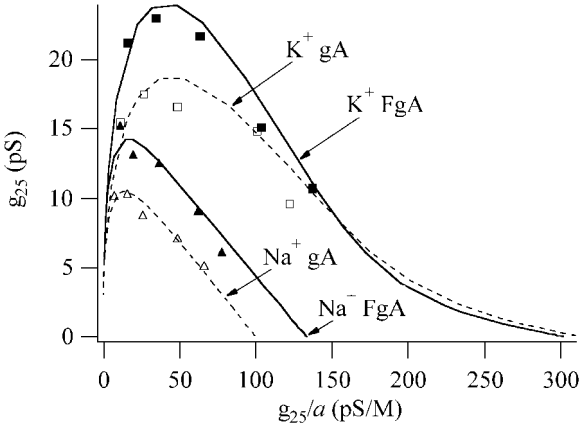

FIGURE 7 Eadie–Hofstee plots, g_{25} versus g_{25}/a (where the small signal conductance, g_{25}, is the conductance at 25 mV and a is the activity of the permeant ion), for the DPhPC data sets. Native gA data are shown as open markers and 5F-Trp_{13} gA data are shown as solid markers for NaCl and KCl salts. Theoretical predictions at discrete activities are shown as dashed curves for native gA data and solid curves for 5F-Trp_{13} gA data with points connected.

From Table 2, it can be seen that the increased negative K_2 slope is fitted by the model mainly by an increase in K and secondarily by a decrease in E. Specifically, second-ion entry, D, is only slightly changed by fluorination (C_D^F = 0.90), whereas second-ion exit, E, is reduced by a factor of C_E^F = 0.72 and translocation, K, is increased by a factor of C_K^F = 2.33, yielding a 1.4-fold increase in the magnitude of the slope.

DISCUSSION

Eight sets of five IVs were fit with the 3B2S model with the goal of determining the effects of Trp_{13} fluorination at indole position 5 on the rate constants in the model. Al-

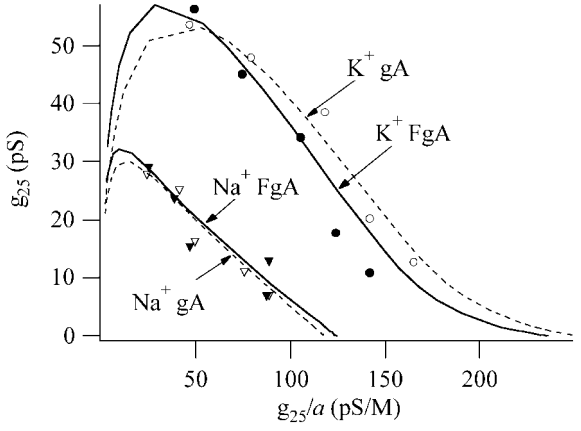

FIGURE 8 Eadie–Hofstee plots, g_{25} versus g_{25}/a (where the small signal conductance, g_{25}, is the conductance at 25 mV and a is the activity of the permeant ion), for the GMO data sets. Symbol meaning as in Fig. 7.

TABLE 3 Comparison to previous fits

	A ($\times 10^6$/Ms)	B ($\times 10^6$/s)	K ($\times 10^6$/s)	D ($\times 10^6$/Ms)	E ($\times 10^6$/s)	α_1	α_2
GMO*/K^+	84.3	2.94	104	115	48.1	0.090	0.206
GMO†/K^+	90	9	45	90	99	0.08	0.23
DPhPC‡/Na^+	61.7	15.6	8.44	20.8	16.1	0.082	0.151
DPhPC§/Na^+	71	24	7	2	23	0.04	0.11

*Current work, (see Tables 1 and 2, basis set with lipid coupling constants).
†From Hladky and Haydon, 1984, Eadie–Hofstee (G-a) fit; V-dependencies for A and B from fit II (see Urban and Hladky 1979).
‡Current work (see Tables 1 and 2, basis set with ion coupling constants).
§From Becker et al., 1992.

though the hope is that these changes can be related to expected electrostatic changes computed independently (Anderson et al., 2001), some assumptions are required, and the uniqueness and robustness of the model must be evaluated. It is assumed that the fluorination does not affect the average position of the Trp$_{13}$ side chain, or does so only as much as has been observed using solid-state NMR in solvent-free DMPC multilayers (Cotten et al., 1999), even though the experiments performed here were done in solvent-inflated GMO and DPhPC bilayers, approximately 8 and 20 Å thicker, respectively. Arguments against large conformational changes were presented previously (Busath et al., 1998), but are not incontrovertible. In addition, we have assumed that changes in the rate constants are exponentially related to appropriately chosen electrostatic potential energies of interaction between the Trp side chain and its bulk dielectric reaction field and the channel contents, i.e., the ion and channel water. This ignores entropic or dynamic averaging affects, which we expect to be negligible, and any inadequacies in the simple Boltzmann factor component of rate theory.

Furthermore, our coupling scheme implicitly assures that fluorination of Trp$_{13}$ will have the same effect on the binding affinity of Na^+ and K^+. We believe that the indole dipole is sufficiently far from the permeation pathway that this is a reasonable assumption for the gA channel, and note that a possibly related change (Markham et al., 2001), responsible for producing the spontaneously occurring ministate, did not change the gA selectivity for alkali metal cations (Busath and Szabo, 1988). There are other assumptions implicit in our coupling scheme and restricted voltage dependencies that may be unjustified, but our purpose here is to demonstrate that 5-flurination can either enhance or inhibit conductance depending on the background free energy profile, which appears to differ for the two ions and, more importantly, for the two lipids (see below). Explorations of the χ_r^2 surface using various initial guesses and with various combinations of constraints (data not shown) indicated that the constraints used do not appreciably bias the outcome.

The parameters of the fit for gA can be compared to previous models. Several groups have used the two-site kinetic model, and many physical measurements of binding and kinetic data have been made that are relevant to the parameters deduced here. It is beyond the scope of this paper to review all of these fits and measurements in detail. Instead, the current gA parameters for GMO bilayers will be compared to those of Hladky and Haydon (1984); and those for DPhPC bilayers will be compared to those of Becker et al., (1992). The comparisons are presented in Table 3, which gives values for the corresponding rate constants and electrical distances. Then, the implications of the fluorination-coupling constants for the energetics will be compared to recently computed electrostatic interaction energies (Anderson et al., 2001). Other comparisons, such as ion–ion interaction effects explored by Jing et al. (1995) and others, will be considered in future work.

Comparison to previous fits

In GMO bilayers with K^+ as the permeant ion, A, D, and the voltage-dependencies are nearly the same in the current fit (Table 3, *first row*) as in that obtained by Hladky and Haydon (1984). However, the first-ion exit rate constant, B, and, to a lesser extent, the second-ion exit rate constant, E, and translocation rate constant, K differ. The first-ion exit rate constant typically varies considerably between fits, sometimes due to a poor definition of the limiting slope in the Eadie–Hofstee plot at low concentrations. The second-ion exit rate constant compensates changes in the first-ion exit rate constant (D. D. Busath, unpublished observation). The translocation and first-ion exit rate constants often interact as seen in Fig. 6, where an increase in the first-ion exit rate constant can be compensated by a decrease in the translocation rate constant. Both the value of B determined here and in the Eadie–Hofstee feature (G-a) fit in Hladky and Haydon (1984) are intermediate (compared to their deep-well and shallow-well models), with equally effective fits being obtained using values for B $\sim$ 4-fold higher or lower.

Becker et al. (1992) fitted Na^+ currents in DPhPC/decane bilayers using both the simple 3B2S model and two elaborations of the model. One elaboration included the increase in concentration of permeable ions near the channel entry due to charging of the membrane capacitance (interfacial

polarization); the other explicitly included ion "diffusion limitation" in the bulk near the channel entry and exit. The elaborations improved the fit slightly for gA currents, but did not for gA mutants where Trp was replaced by Phe. Nevertheless, it was demonstrated that the simpler 3B2S model in which the elaborations were just considered part of a compound entry or exit step could closely fit the currents. It can be seen that the fitted parameters in the simple model are quite similar to the ones reported here. For instance, in DPhPC bilayers with Na^+ as the permeant ion, A, B, K, and E are nearly the same in the current fit (Table 3, *third row*) as in that obtained in Becker et al. (1992). There are modest differences in the voltage dependencies, and the second-ion entry rate constant, D, differs markedly in the two fits.

The difference between the Becker et al. (1992) value for D and that of the current fit probably reflects different methods of fitting Na^+ data, given the relative lack of inflection point in the Eadie–Hofstee plot, i.e., a different local minimum in the two different data sets. The very low value of D in the Becker et al. (1992) fit strongly limits double occupancy, and thus flux coupling, which would produce a low flux ratio exponent ($\sim$1.0). The parameter set reported here produces a maximum flux ratio exponent of 1.18 at $\sim$1 M and of 1.10 at 0.1 M Na^+ (computations not shown). These values can be compared to the value of 1.2 measured for 0.1 M Na^+ in ox brain lipids (Schagina et al., 1983). However, the negative surface charge on the ox brain lipid membranes may enhance double occupancy, and a lower value (1.0) has been measured in neutral lipids (Procoppio and Andersen, 1979; Hladky, 1999). Our values are somewhat more consistent with evidence of Na^+ double occupancy in ^{13}C-NMR studies (Jing et al., 1995). However, given our coupling assumptions and the lack of features in the Na^+ data set, our parameters for Na^+ should not be viewed as definitive. Interestingly, under all four conditions of lipid and ion species, the models presented here predict that 5-fluorination of Trp_{13} should increase the maximum flux ratio exponent by $\sim$10% (computations not shown), presumably due to the reduction of the translocation barrier (Hille and Schwarz, 1978).

The predictions of the present model for currents in 1.0 M Na^+ at membrane potentials between 200 and 500 mV in DPhPC bilayers (computations not shown) are reasonably consistent with measurements made by others (Becker et al., 1992). However, the model predicts a shift to superlinear IV in this voltage range for 0.1 M salts, unlike the continued sublinearity observed by Andersen (1983), perhaps reflecting inadequate enforcement of diffusion limitation in these extreme conditions.

TABLE 4 Comparison to electrostatic prediction

	C_A^F/C_B^F	C_D^F/C_E^F	C_K^F
3B2S fit	1.13	1.26	2.33
Electrostatic prediction*	1.05	N.D.	2.45

*From Anderson et al., 2001.

Comparison to electrostatics calculations

Although the parameters are not identical to these previous fits, we suppose that our simultaneous fit of eight experimental paradigms with coupled parameter sets represents a greater restraint on the fit, and, therefore, that the current parameter set may be somewhat more reliable. Furthermore, the finding that the fitting algorithm converged three times to the same parameter set from very different starting parameter sets indicates that the result is robust for the current data set. Therefore, we next compare the fluorination-coupling constants to computed changes in the potential energies of interaction performed using CHARMM with ab initio charges for the Trp_{13} and 5F-Trp_{13} (Anderson et al., 2001). Note that the coupling constants represent the ratio of rate constants for fluorinated peptide to native, and thus directly reflect differences in free energy barriers for the different transport steps. We select for this purpose the potential changes computed with no changes in the side chain position. Position changes of the magnitude measured in DMPC bilayers are shown in Anderson et al., (2001) to have modest effects on the energy changes. The comparison is made by assuming a Boltzmann factor dependence in the rate constants,

$$\frac{C_A^F}{C_B^F} = \exp\{-(E_4^F - E_4)/RT\},$$

$$C_K^F = \exp\{-[(E_0^F - E_0) - (E_4^F - E_4)]/RT\}. \quad (5)$$

Here the coupling constants denote (as in Table 1) the effect of fluorination on the rate constant. E_4 and E_0 are the interaction energies between side chains (and their reaction fields) with ion (and channel waters) interpolated to 9.3 Å from the channel center (near the ion binding site) and at the channel center, respectively. The superscripted versions represented the interaction energies computed with the fluorinated Trp side chain. The interaction energies were not estimated for ions at a point that could be stated to represent the entry/exit barrier, so only the effects on the binding affinity are considered here. However, it could be argued that effects of side-chain fluorination in the bath should be largely shielded by the bath, so that ion entry rates should be mostly unaffected. Table 4 presents the comparison between the fit and the electrostatics computation based on Eqs. 5. The electrostatics computation predicts both that fluorination will enhance the translocation rate constant, as represented by the increase in C_K^F, and that it will increase the binding affinity of the ion binding site, shown by the increase in C_A^F/C_B^F. From the fit, the fluorination-induced reduction in effective translocation-barrier energy is 0.50 kcal/mol and the fluorination-increased binding-site energy

is 0.07 kcal/mol, compared to computed values of 0.527 and 0.026 kcal/mol, respectively (Anderson et al., 2001). We consider this to be reasonable agreement between the two theories. The effect of fluorination on second-ion binding is somewhat greater than the effect on first-ion binding according to the fit, but no electrostatic computations are yet available for comparison.

As a side note, it should also be pointed out that there is a large difference between GMO and DPhPC current measurements in the K_2 region slope of the Eadie–Hofstee plots, which were adequately fitted in the 3B2S model, deriving primarily from a 5.62-fold increase in translocation rate constant, K, in GMO bilayers (see C_K^{Lipid} in Table 2). The physical origin of this difference is likely to be the difference in interfacial dipole potential between the two lipids. Monolayer surface potentials have been measured for various lecithins, expected to be similar in head group structure to DPhPC, and for GMO (Pickar and Benz, 1978). For instance, the difference between dioleoylphosphatidyl choline and GMO surface potentials is 116 mV. Some of this difference applies to the binding energy as well, reducing the effect on the translocation barrier, and some attenuates due to the dielectric shielding of the channel walls and contents (Jordan, 1983). The lipid-coupling constant can be used to estimate the projection of the interfacial dipole potential difference onto the translocation barrier, ΔV, using the equation

$$\Delta V = \frac{RT}{FZ} \ln C_K^{Lipid}, \quad (6)$$

where R, T, F, and z have their usual thermodynamic meanings. Based on Eq. 6, the central barrier is higher in DPhPC bilayers due to an electrical potential increase of 44.2 mV, consistent with the interfacial dipole potential difference, given its expected attenuation by a factor of $\sim$2 (Jordan, 1983).

Within the context of this 3B2S kinetic model, then, the explanation previously offered for the lack of an effect of Trp$_{13}$ fluorination on gA conductance in GMO bilayers (Busath et al., 1998), namely that conductance is insensitive to changes in translocation because translocation is not rate limiting, seems adequate. However, in contrast to the suggestion presented there for the fluorination-induced reduction in conduction in GMO bilayers, we note that exit, rather than entry, is rate limiting according to the present 3B2S model in the intermediate concentration range (see Table 2). The inhibition of exit by fluorination, as evident in the increased ion binding affinity and corroborated with the electrostatic calculations (see Table 4, also C_B^F and C_E^F in Table 2), appears to be the primary mechanism of fluorination-induced reduction of gramicidin conductance in GMO bilayers.

SUMMARY

According to kinetic modeling of a 320-point data set, fluorination affected the channel energy profile by reducing the activation energy needed for translocation, slightly increasing the activation energy for exit, and left the activation energy needed for entry relatively unchanged. The coupled parameters indicate free energy changes of -0.50 kcal/mol for the translocation barrier and -0.07 kcal/mol for the free energy of binding, reasonably consistent with potential energies computed using molecular mechanics reported in the companion paper (Anderson et al., 2001). From the modeling, it appears that, in the 0.1–1.0 M ion concentration range, 5F-Trp$_{13}$ gA currents are increased in DPhPC bilayers due to an increased translocation rate constant and are slightly decreased in GMO bilayers due to a small decrease in the ion exit rate constant.

We thank Dean Anderson for providing the computed interaction energies used in Table 4 and Prof. Mark F. Schumaker for helpful comments.

This project was supported by National Institutes of Health grant R01 AI23007 to T.A.C. and D.D.B.

REFERENCES

Andersen, O. S. 1983a. Ion movement through gramicidin A channels. Single-channel measurements at very high potentials. *Biophys. J.* 41: 119–133.

Andersen, O. S. 1983b. Ion movement through gramicidin A channels. Interfacial polarization effects on single-channel current measurements. *Biophys. J.* 41:135–146.

Andersen, O. S. 1983c. Ion movement through gramicidin A channels. Studies on the diffusion-controlled association step. *Biophys. J.* 41: 147–165.

Andersen, O. S. 1999. Editorial: Graphic representation of the results of kinetic analysis. *J. Gen. Physiol.* 114:589–590.

Anderson, D. G., R. B. Shirts, T. A. Cross, and D. D. Busath. 2001. Non-contact dipole effect on channel permeation. V. Computed potentials for fluorinated gramicidin. *Biophys. J.* 81:1255–1264.

Becker, M. D., R. E. Koeppe, II, and O. S. Andersen. 1992. Amino acid substitutions and ion channel function. Model-dependent conclusions. *Biophys. J.* 62:25–27.

Bevington, P. R. 1969. Data Reduction and Error Analysis for the Physical Sciences. McGraw-Hill, Inc., New York. 1–8, 187–188.

Busath, D. D. 1993. The use of physical methods in determining gramicidin channel structure and function. *Annu. Rev. Physiol.* 55:473–501.

Busath, D., and G. Szabo. 1988. Permeation characteristics of gramicidin conformers. *Biophys. J.* 53:697–707.

Busath, D. D., C. D. Thulin, R. W. Hendershot, L. R. Phillips, P. Maughn, C. D. Cole, N. C. Bingham, S. Morrison, L. C. Baird, R. J. Hendershot, M. Cotten, and T. A. Cross. 1998. Non-contact dipole effects on channel permeation. I. Experiments with (5F-indole)Trp-13 gramicidin A channels. *Biophys. J.* 75:2830–2844.

Cooper, K. E., P. Y. Gates, and R. S. Eisenberg. 1988. Diffusion theory and discrete rate constants in ion permeation. *J. Membr. Biol.* 106:95–105.

Cotten, M., C. Tian, D. D. Busath, R. B. Shirts, and T. A. Cross. 1999. Modulating dipoles for structure–function correlations in the gramicidin A channel. *Biochemistry.* 38:9185–9197.

Dorigo, A. E., D. G. Anderson, and D. D. Busath. 1999. Noncontact dipole effects on channel permeation. II. Trp conformations and dipole potentials in gramicidin A. *Biophys. J.* 76:1897–1908.

Eisenman, G., and J. P. Sandblom. 1983. Energy barriers in ionic channels: data for gramicidin A interpreted using a single-file (3B4S″) model having 3 barriers separating 4 sites. *In* Physical Chemistry of Transmembrane Ion Motions. G. Spach, editor. Elsevier, Amsterdam. 329–348.

Hainsworth, A. H., and S. B. Hladky. 1987. Gramicidin-mediated currents at very low permeant ion concentrations. *Biophys. J.* 52:109–113.

Hille, B., and W. Schwarz. 1978. Potassium channels as multi-ion single-file pores. *J. Gen. Physiol.* 72:409–442.

Hinton, J. F., J. Q. Fernandez, D. C. Shungu, and F. S. Millet. 1988. T1–205 NMR determination of the thermodynamic parameters for the binding of monovalent cations to gramicidins A and C. *Biophys. J.* 55:527–533.

Hladky, S. B. 1984. Ion currents through pores. The roles of diffusion and external access steps in determining the currents through narrow pores. *Biophys. J.* 46:293–297.

Hladky, S. B. 1999. Can we use rate constants and state models to describe ion transport through gramicidin channels? *In* Proceedings of the Novartis Foundation Symposium No. 225: Gramicidin and Related Ion Channel-Forming Peptides. John Wiley & Sons, Ltd. Chichester, UK. 93–107.

Hladky, S. B., and D. A. Haydon. 1984. Ion movements in gramicidin channels. *Curr. Topics Membr. Transp.* 21:327–372.

Jing, N., K. U. Prasad, and D. W. Urry. 1995. The determination of binding constants of micellar-packaged gramicidin A by ^{13}C- and ^{23}Na-NMR. *Biochim. Biophys. Acta.* 1238:1–11.

Jordan, P. C. 1983. Electrostatic modeling of ion pores. II. Effects attributable to the membrane dipole potential. *Biophys. J.* 41:189–195.

Kramers, H. A. 1940. Brownian motion in a field of force and the diffusion model of chemical reactions. *Physica.* 7:284–304.

Levitt, D. G. 1982. Comparison of Nernst–Plank and reaction-rate models for multiply occupied channels. *Biophys. J.* 37:575–587.

Markham, J. C., J. A. Gowen, T. A. Cross, and D. D. Busath. Comparison of gramicidin A and gramicidin M channel conductance dispersities. *Biochim. Biophys. Acta.* In press.

McBride, D. W. 1981. Anomalous mole fraction behavior, momentary block, and lifetimes of gramicidin A in silver and potassium fluoride solutions. Doctoral dissertation. Univ. of California Los Angeles.

Pickar, A. D., and R. Benz. 1978. Transport of oppositely charged lipophilic probe ions in lipid bilayer membranes having various structures. *J. Membr. Biol.* 44:353–376.

Press, W. H., B. P. Flannery, S. A. Teukolsky, and W. T. Vetterling. 1986. Numerical Recipes, The Art of Scientific Computing. Cambridge University Press, Cambridge, UK. 523–546.

Procopio, J., and O. S. Andersen. 1979. Ion tracer fluxes through gramicidin A modified lipid bilayers. *Biophys. J.* 28:8 (abstr).

Schagina, L. V., A. E. Grinfeldt, and A. A. Lev. 1983. Concentration dependence of bidirectional flux ratio as a characteristic of transmembrane ion transporting mechanism. *J. Membr. Biol.* 73:203–216.

Thompson, G., N. Thompson, M. Cotten, T. A. Cross, and D. D. Busath. 1999. Kinetic modeling of 5F-Trp_{13} gramicidin A channel currents. *Biophys. J.* 76:A444.

Wang, K.-W., S. Tripathi, and S. B. Hladky. 1995. Ion binding constants for gramicidin A obtained from water permeability measurements. *J. Membr. Biol.* 143:247–257.

Urban, B. W., and S. B. Hladky. 1979. Ion transport in the simplest single file pore. *Biochim. Biophys. Acta.* 554:410–429.